

Article

Chemisorption and Surface Reaction of Hafnium Precursors on the Hydroxylated Si(100) Surface

Truong Ba Tai ¹, Jonghun Lim ^{2,*} and Hyeyoung Shin ^{1,*}

¹ Graduate School of Energy Science and Technology (GEST), Chungnam National University, Daejeon 34134, Republic of Korea; taib.truong@gmail.com

² Department of Environment and Energy Engineering, Sungshin Women's University, Seoul 01133, Republic of Korea

* Correspondence: jlim@sungshin.ac.kr (J.L.); shinhy@cnu.ac.kr (H.S.)

Abstract: Hafnium oxide (HfO₂) is widely recognized as one of the most promising high-*k* dielectric materials due to its remarkable properties such as high permittivity, wide band gap, and excellent thermal and chemical stability. The atomic layer deposition (ALD) of HfO₂ has attracted significant attention in recent decades since it enables uniform and conformal deposition of HfO₂ thin films on various substrates. In this study, we examined the initial surface reactions of a series of homoleptic hafnium precursors on hydroxylated Si(100) surfaces using density functional theory calculations. Our theoretical findings align with previous experimental studies, indicating that hafnium amides exhibit higher reactivity compared to other precursors such as hafnium alkoxides and hafnium halides in surface reactions. Interestingly, we found that the chemisorption and reactivity of hafnium precursors are considerably affected by their thermal stability and size. For alkoxide precursors, which have similar thermal stabilities, the size of alkoxide ligands is an important factor in determining their reactivity. Conversely, the reactivity of hafnium halides, which have ligands of similar sizes, is primarily governed by their thermal stability. These insights are valuable for understanding the surface reaction mechanisms of precursors on hydroxylated Si(100) surfaces and for designing new materials, particularly heteroleptic precursors, in future research.

Keywords: density functional theory; hafnium oxide; atomic layer deposition; surface reaction; reaction mechanism



Citation: Tai, T.B.; Lim, J.; Shin, H. Chemisorption and Surface Reaction of Hafnium Precursors on the Hydroxylated Si(100) Surface. *Coatings* **2023**, *13*, 2094. <https://doi.org/10.3390/coatings13122094>

Academic Editor: Mikhail Rodionovich Baklanov

Received: 8 November 2023

Revised: 3 December 2023

Accepted: 10 December 2023

Published: 16 December 2023

Correction Statement: This article has been republished with a minor change. The change does not affect the scientific content of the article and further details are available within the backmatter of the website version of this article.



Copyright: © 2023 by the authors. Licensee MDPI, Basel, Switzerland. This article is an open access article distributed under the terms and conditions of the Creative Commons Attribution (CC BY) license (<https://creativecommons.org/licenses/by/4.0/>).

1. Introduction

Atomic layer deposition (ALD) is a cutting-edge technology for growing thin films, utilizing self-limiting reactions between reactants and substrate surfaces [1]. This process involves repeating sequences of two half-cycles, consisting of a reactant pulse and a subsequent inactive purging step. The self-limiting nature of ALD facilitates the production of high-quality thin films, allowing precise control over their thickness, conformality, and morphology at the molecular level [2,3]. Given these advantages, it is not surprising that both academia and industry have shown significant interest in ALD over the past few decades [4–9]. Nowadays, this technology is utilized in various applications, including microelectronics, solar cells, catalysts, and optical devices [6–8].

Recently, the replacement of silicon oxide (SiO₂) with high-*k* dielectric materials in microelectronic technology has gained increasing attention [10–12]. Among these materials, hafnium oxide (HfO₂) is one of the most promising candidates owing to its superior properties, such as high permittivity, wide band gap, and thermal and chemical stability [13,14]. Significant research efforts have been devoted in recent decades to producing high-performance HfO₂ thin films on Si substrate surfaces using ALD technology. Several types of precursors have been explored, including hafnium halides [15–24], hafnium amides [25–38], hafnium alkoxides [39–41], and heteroleptic precursors based on cyclopentadienyl (Cp) [42,43]. Among them, hafnium chloride (HfCl₄) and hafnium amides are the

most widely used precursors in both academia and industry. HfCl_4 , known for its thermal stability and ease of use in industrial applications, has the disadvantage of having corrosive byproducts that can damage equipment. In contrast, hafnium amides are considered one of the most promising families of organometallic precursors for HfO_2 ALD due to their high reactivity, non-corrosiveness, and suitability for low-temperature processes. Hafnium alkoxide precursors are an interesting alternative, offering moderate reactivity and thermal stability, and are cost-effective and safe for the ALD processes.

Despite numerous experimental studies on the HfO_2 ALD, a comprehensive understanding of the process is still limited. This limitation primarily arises from the fact that the performance of HfO_2 thin films produced via ALD is influenced by a myriad of experimental factors. In this context, modeling studies have proven to be advantageous. Nowadays, theoretical studies utilizing density functional theory (DFT) are extensively employed in material science and engineering [9,38,44]. DFT simulations provide highly accurate theoretical results with minimal variance in reproducibility. Furthermore, DFT modeling is particularly useful for gaining insights into the reaction mechanism of surface reactions and the chemical and physical properties of systems at the molecular level, which can be challenging in experimental studies.

However, it is surprising that theoretical investigations into the HfO_2 ALD process are scarce in the literature, despite the considerable potential of this technique [45–49]. Using a cluster model in which the silicon (Si) surface is represented by Si_nH_m atomic clusters, Zhang and his coworkers [45] explored the reaction mechanism of HfO_2 ALD using HfCl_4 and water as precursors. Wang and his colleagues [46,47] conducted a DFT study of HfO_2 ALD with a tetrakis (ethylmethylamino) hafnium (TEMAH) precursor by simulating the Si surface with a Si_9H_{12} cluster. The cluster model, however, has several limitations in representing surface reactions, primarily because it heavily depends on the cluster size and does not fully simulate the surface environment. Therefore, the application of theoretical investigations using periodic boundary condition DFT methods in the HfO_2 ALD process becomes essential, as these methods are likely to produce predictions that more closely align with the experimental outcomes.

In a recent study, we investigated the reaction mechanism of the HfO_2 ALD process using TEAMH and water [38], employing DFT calculations. Our research provided deeper insights into the conversion of TEAMH into a Hf atom on the hydroxylated Si(100) surface. To further understand the influence of different ligands on the reactivity of homoleptic hafnium precursors, we performed a systematic study on the chemisorption in HfO_2 ALD, using DFT calculations. It is known that chemisorption, usually occurring during the first ligand exchange reaction between the precursors and the surface, is crucial for the efficacy of ALD processes. We analyzed nine homoleptic hafnium precursors, including hafnium alkoxides, hafnium halides, and hafnium amides. Intriguingly, our theoretical findings reveal a correlation between the thermal stability of these precursors and their surface reactivity. Additionally, these computational results show good agreement with experimental data. Among the nine precursors examined, the energy barriers for the surface reaction of hafnium amides range from 7.1 kJ/mol to 28.4 kJ/mol, significantly lower than those for hafnium alkoxides and hafnium halides. This finding helps explain why the HfO_2 ALD process with hafnium amide precursors is feasible at lower temperatures compared to other precursors.

2. Computational Methods

Spin-polarized density functional theory (DFT) calculations were carried out using the project augmented wave (PAW) method [50], as implemented in the Vienna ab initio simulation package (VASP) [51–53]. The Perdew–Burke–Ernzerhof (PBE) functional was employed to obtain the exchange and correlation energies within the generalized gradient approximate (GGA) framework [54]. The electronic wave functions were expanded in a plane-wave basis set with a kinetic energy cutoff of 400 eV. The force convergence criteria were set at 0.01 eV/Å for ionic relaxations and 0.05 eV/Å for transition state searches,

respectively, while the energy convergence criterion for the electronic self-consistency loop was established at 0.01 meV. The transition states were examined using the climbing-image nudged elastic band (CI-NEB) method [55,56] which involves seven images per search. A (3 × 3) supercell model of the fully hydroxylated Si(100) surface was used. The Si atoms in the bottom layer were passivated by H atoms. The two bottom Si layers and their terminating H atoms were kept fixed, while others were allowed to relax during simulations. A more detailed description of the surface model can be found in our recent report [38]. For the surface calculations, a (3 × 3 × 1) Monkhorst–Pack [57] k-point mesh was applied, with no symmetry constraints and a dipole correction was included. Long-range dispersion interactions were accounted for by incorporating dispersion corrections calculated via the DFT-D3 method [58] into the DFT energies. The images of configurations were generated using VESTA (Version 3, Koichi Momma and Fujio Izumi, Ibaraki City, Japan) [59] and Mercury (Version 3.8, Cambridge Crystallographic Data Center, Cambridge City, UK) [60] visualization software.

To evaluate the thermal stability of the precursors, their bond dissociation energies (BDEs) were calculated using the isolated molecular models. The BDEs for the hafnium alkoxides (Hf[OR]₄) and hafnium halides (HfX₄) are defined as the energy required to dissociate a chemical bond between hafnium and alkoxide groups (in hafnium alkoxides) or hafnium and halide groups (in hafnium halides). These processes are represented in Equations (1) and (2).



All electronic structure calculations for the isolated molecular models were performed using Gaussian 16 [61] programs. Geometry optimizations and calculations of harmonic vibrational frequencies for the hafnium precursors, both in neutral and radical states, were fully conducted using the hybrid PBE0 functional [62]. These calculations were coupled with the 6-31G(d,p) basis set [63] for light elements (carbon (C), hydrogen (H), and oxygen (O)), and the def2sv basis set [64] for halogens and hafnium (Hf). As detailed in Table S1, to verify the accuracy of the results obtained with the def2sv basis set, additional calculations were carried out for hafnium halides using larger basis sets. These included aug-cc-pVTZ for fluorine (F) [65] and chlorine (Cl) [66], and aug-cc-pVTZ-PP for Hf [67] and iodine (I) [68,69]. The aug-cc-pVTZ-PP basis sets for Hf and I were sourced from EMSL/PNNL Basis Set Exchange [70–72]. Structural images of the precursors were generated using Chemcraft software (Version 1.8, Grigoriy A. Andrienko, <https://www.chemcraftprog.com> access on 1 December 2023) [73]. (Figure S1)

3. Results and Discussion

3.1. Chemisorption and Surface Reaction of Hafnium Alkoxide Precursors

Metal alkoxide precursors (M[OR]_n), where a central metal (M) is directly bonded to alkoxide ligands (-OR) have attracted significant interest in metal oxide ALD research [39–41]. These precursors typically exhibit moderate reactivity along with high volatility, thermal stability, and safety. Owing to their relatively high thermal stability and volatility, metal alkoxides containing bulky ligands, such as isopropoxide (M[OⁱPr]₄) and tert-butoxide (M[O^tBu]₄), are commonly employed as homoleptic alkoxide precursors in previous experimental studies on HfO₂ ALD [39–41]. Mui and Musgrave carried out a DFT study on the reaction mechanisms of HfO₂ ALD using hafnium ethoxide (Hf[OEt]₄) and water as reactants, employing an isolated molecular model in gas phase [48]. However, the chemisorption and their structural characteristics on the surface have not been studied in detail since the model did not consider the interaction between the Si surface and reactants. In this work, we performed periodic condition DFT calculations to analyze the chemisorption and surface reaction of a series of hafnium alkoxides, including hafnium methoxide (Hf[OMe]₄), hafnium isopropoxide (Hf[OⁱPr]₄) and hafnium tert-butoxide (Hf[O^tBu]₄) on the hydroxylated Si(100) surface.

3.1.1. Hafnium Methoxide Precursor

As shown in Figure 1, hafnium methoxide ($\text{Hf}[\text{OMe}]_4$) initially adsorbs onto the hydroxylated $\text{Si}(100)$ surface with an adsorption energy of -126.0 kJ/mol. This exothermic chemical adsorption forms a new bond between the Hf atom of $\text{Hf}[\text{OMe}]_4$ and the O atom of surface hydroxyls (OH) (**1a**). The bonding length is 2.28 Å, slightly longer than the average Hf-O bond distance (1.95 Å) in the free precursor $\text{Hf}[\text{OMe}]_4$.

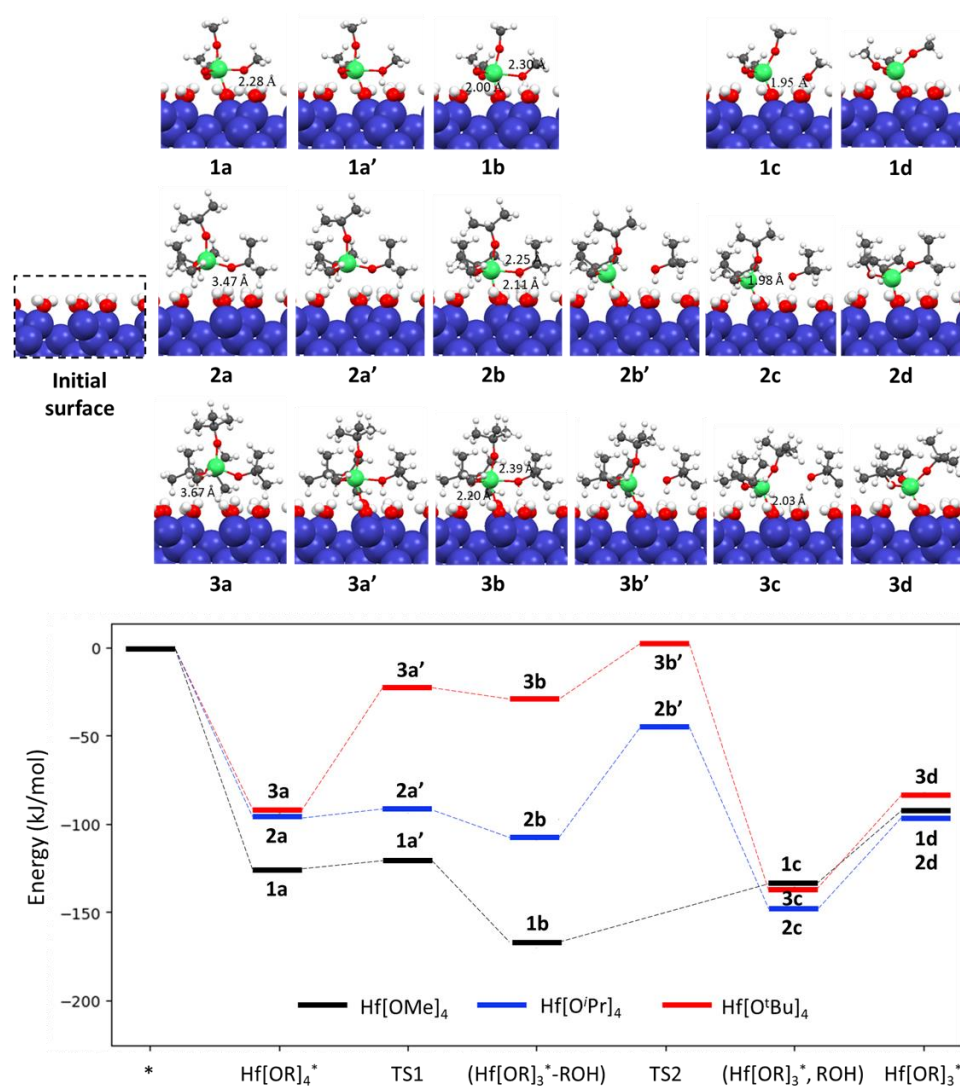


Figure 1. Reaction energy profiles in kJ/mol for chemisorption and surface reactions of hafnium alkoxides ($\text{Hf}[\text{OR}]_4$) on the fully hydroxylated $\text{Si}(100)$ surface. Blue, red, white, gray and green balls indicate Si, O, H, C, and Hf atoms, respectively.

The first ligand exchange reaction converts the adsorbed $\text{Hf}[\text{OMe}]_4$ (**1a**) into an intermediate (**1b**), via a transition state (**1a'**), and then into an adsorbed hafnium tri-methoxide ($\text{Hf}[\text{OMe}]_3$) (**1c**). This step is an exothermic process with a small activation energy of 5.4 kJ/mol, leading to the formation of the intermediate (**1b**). The intermediate (**1b**) is a stable complex in which a methanol molecule remains weakly bonded to the adsorbed $\text{Hf}[\text{OMe}]_3$, forming a $\text{Hf}[\text{OMe}]_3\text{-MeOH}$ complex. The configuration of intermediate (**1b**), depicted in Figure 1, reveals demonstrated that the MeOH molecule is bonded to the Hf atom in $\text{Hf}[\text{OMe}]_3$ through an Hf-O bond with a length of 2.30 Å. This bond length is 0.30 Å longer than the distance between the Hf atom in the $\text{Hf}[\text{OMe}]_3\text{-MeOH}$ and the O atom of the OH group on the hydroxylated $\text{Si}(100)$ surface.

The dissociation of methanol (MeOH) from **1b**, leading to the formation of state **1c** where one methanol is adsorbed onto the surface, is an endothermic process. This step occurs without a transition state and has a dissociation energy of 33.0 kJ/mol. This energy change reduces the distance between the Hf atom in Hf[OMe]₃ and the O atom of the surface OH group from 2.00 Å to 1.95 Å. Subsequently, the methanol molecule desorbs from the Si(100) surface, resulting in the final configuration, **1d**, with an endothermic desorption energy of 41.0 kJ/mol. It is noteworthy that this overall surface reaction process involves the breaking of two chemical bonds: Hf-OMe bond in the precursor Hf[OMe]₄ and a H-O bond in the surface OH group. As a result, a new Hf-O chemical bond is formed between the Hf atom of the adsorbed Hf[OMe]₃ and a surface O atom, with methanol released as a byproduct. Overall, the entire process is exothermic, with a net energy release of −87.5 kJ/mol.

3.1.2. Hafnium Isopropoxide Precursor

Figure 1 also presents the adsorption configuration of hafnium isopropoxide (Hf[OⁱPr]₄) on a hydroxylated Si(100) surface, along with the transition, intermediate, and final states of the ligand exchange reaction that transforms the adsorbed Hf[OⁱPr]₄ into adsorbed hafnium tri-isopropoxide (Hf[OⁱPr]₃). The steric effects of the bulky isopropoxide groups result in a Hf-O distance of 3.47 Å between the Hf atom of the adsorbed Hf[OⁱPr]₄ (**2a**) and the O atom of the surface OH. This distance is significantly longer than the 2.28 Å observed for Hf[OMe]₄ (**1a**), leading to physisorption without the formation of a Hf-O bond.

The ligand exchange reaction that converts the adsorbed Hf[OⁱPr]₄ into the final product, adsorbed Hf[OⁱPr]₃, occurs in two-steps. In the first step, the adsorbed Hf[OⁱPr]₄ (**2a**) readily transforms into a stable intermediate complex (**2b**), via a transition state (**2a'**) with a small activation energy of 3.0 kJ/mol. The configuration of complex **2b** shows that the Hf-O distance between the O atom of the resulting isopropanol and the Hf atom is 2.25 Å, only 0.14 Å longer than the Hf-O bond length between the Hf atom and the surface oxygen (2.11 Å). In the second step, an exothermic reaction occurs, but with a high activation energy of 63.8 kJ/mol (**2b'**). The Hf-O bond length between the Hf atom and the surface O atom decreases from 2.11 Å in the intermediate complex **2b** to 1.98 Å in the final product (**2c**), as shown in Figure 1. In the final step, isopropanol is released from the surface, and a covalent bond is formed between the Hf atom of Hf[OⁱPr]₃ and the surface O-atom.

3.1.3. Hafnium Tert-Butoxide Precursor

Similar to the Hf[OⁱPr]₄ precursor, hafnium tert-butoxide (Hf[O^tBu]₄) features large-sized tert-butoxide ligands, resulting in the physisorption of Hf[O^tBu]₄ on the hydroxylated Si(100) surface. In the physisorption configuration **3a**, shown in Figure 1, the Hf-O distance between the Hf atom of the precursor Hf[O^tBu]₄ and the O atom of the surface hydroxyl is 3.67 Å, similar to that observed for Hf[OⁱPr]₄.

The transformation of adsorbed Hf[O^tBu]₄ into hafnium tri-tert-butoxide (Hf[OBu]₃) also involves two steps. The first step is the conversion of adsorbed Hf[OBu]₄ (**3a**) into an intermediate (**3b**), characterized by a high energy barrier of 70.2 kJ/mol. In this intermediate, the distance between the O atom of tert-butanol and the Hf atom is 2.39 Å, sufficient to break their Hf-O bond. The second step leads to the formation of hafnium tri-tert-butoxide (**3c**) and primarily involves a configuration rearrangement, with an activation energy of 34.1 kJ/mol. This value is significantly lower than the 63.8 kJ/mol observed in the second step for Hf[OⁱPr]₄. Ultimately, tert-butanol is released from surface and a covalent bond is formed between the Hf atom of hafnium tri-tert-butoxide and a surface O atom.

Our computational results indicate that hafnium methoxide, with its smaller-sized ligands, can form a Hf-O chemical bond between the Hf atom of the precursor and the surface OH group in the first step (as seen in **1a**, Figure 1). This leads to a low energy barrier of 5.4 kJ/mol in the subsequent chemisorption steps. In contrast, for other alkoxide precursors with larger ligands, only hydrogen bonds between the alkoxide groups and

surface hydroxyl groups were observed, mainly contributing to their adsorption energies on the surfaces. Consequently, their following chemisorption exhibited revealed much higher energy barriers (63.8 kJ/mol for Hf[O^tPr]₄ and 70.2 kJ/mol for Hf[O^tBu]₄).

3.2. Chemisorption and Surface Reaction of Hafnium Halide Precursors

Hafnium halides are recognized as highly promising precursors for HfO₂ ALD, owing to their notable thermal stability and low impurity levels. Over the past decades, several experimental studies employing these precursors have been conducted. In order to gain a deeper understanding of the reactivity and chemisorption characteristics of hafnium halides on the hydroxylated Si(100) surface, we performed DFT calculations on a series of these compounds, encompassing hafnium iodide (HfI₄), hafnium chloride (HfCl₄), and hafnium fluoride (HfF₄).

3.2.1. Hafnium Iodide Precursor

Our calculations indicated that hafnium iodide (HfI₄) is adsorbed onto the hydroxylated Si(100) surface and forms a new bond with a surface hydroxyl group, with an adsorption energy of −104.9 kJ/mol. In the preferred adsorption configuration **4a** (as shown in Figure 2), hafnium exhibits a stable five-fold coordination state in which it is bound to four I atoms and one O atom of the surface hydroxyl. The ligand exchange reaction results in the formation of the final state, hafnium tri-iodide (HfI₃) **4b**, and releases one molecule of HI (also shown in Figure 2). In this ligand exchange process, the HI molecule is generated through the interaction between an I-atom from adsorbed HfI₄ and a hydrogen atom from the surface OH-group. The Hf-O distance between the Hf atom and the surface oxygen is reduced from 2.23 Å for **4a** to 1.89 Å for **4b**. This reaction is exothermic, with an energy barrier of 71.4 kJ/mol through a transition state **4a'**. Interestingly, the hafnium atom in the state **4b** retains a five-fold coordination state in which hafnium is bound to three I atoms, one surface O atom, and one O atom of a neighboring hydroxyl group. Removing free HI from the surface via desorption has a small desorption energy of 23.1 kJ/mol.

3.2.2. Hafnium Chloride Precursor

It is interesting to show that the precursor HfCl₄ is adsorbed onto the hydroxylated Si(100) surface with a large adsorption energy of 147.6 kJ/mol, resulting in a six-fold coordinate state for the Hf-atom (as depicted in image **5a**, Figure 2). The adsorption energy of HfCl₄ on the hydroxylated Si surface was reported to be 73.1 kJ/mol by Zhang et al. [45], in which HfCl₄ only interacts with one OH group. This difference can be understood by the fact that the authors used a cluster model Si₉O₃H₁₂-OH in which only one OH group was available. The Hf-O distances between the Hf atom and the O atoms of the surface hydroxyl groups were 2.31 Å and 2.36 Å.

The adsorption configuration **5a** undergoes a ligand exchange reaction, resulting in the formation of hafnium tri-chloride (HfCl₃) **5b** through a transition state **5a'** (as shown in Figure 2). The activation energy of this reaction is 76.1 kJ/mol, which is comparable to the value of 71.4 kJ/mol found for HfI₄. The Hf-O bonding length between the Hf atom and the surface O atom is reduced from 2.31 Å for **5a** to 1.89 Å for **5b**, while a small change of 0.05 Å is observed for the Hf-O distance between the Hf atom and the neighboring OH group of **5a** and **5b** (from 2.36 Å to 2.31 Å). Free HCl is removed from surface via desorption which is 14.1 kJ/mol endothermic.

3.2.3. Hafnium Fluoride Precursor

Similar to the hafnium chloride precursor, hafnium fluoride HfF₄ is adsorbed on the hydroxylated Si(100) surface and forms two chemical bonds with two surface OH groups (image **6a**, Figure 2). The adsorption energy is −192.1 kJ/mol, which is considerably higher than that of HfCl₄ and HfI₄. The adsorbed HfF₄ **6a** is converted into the state **6b** through a transition state **6a'**, with a high energy barrier of 97.4 kJ/mol. In the configuration **6b**, the

Hf-O bond between the Hf atom and the surface O atom is reduced by 0.32 Å compared to the initial configuration 6a and is 1.97 Å in length.

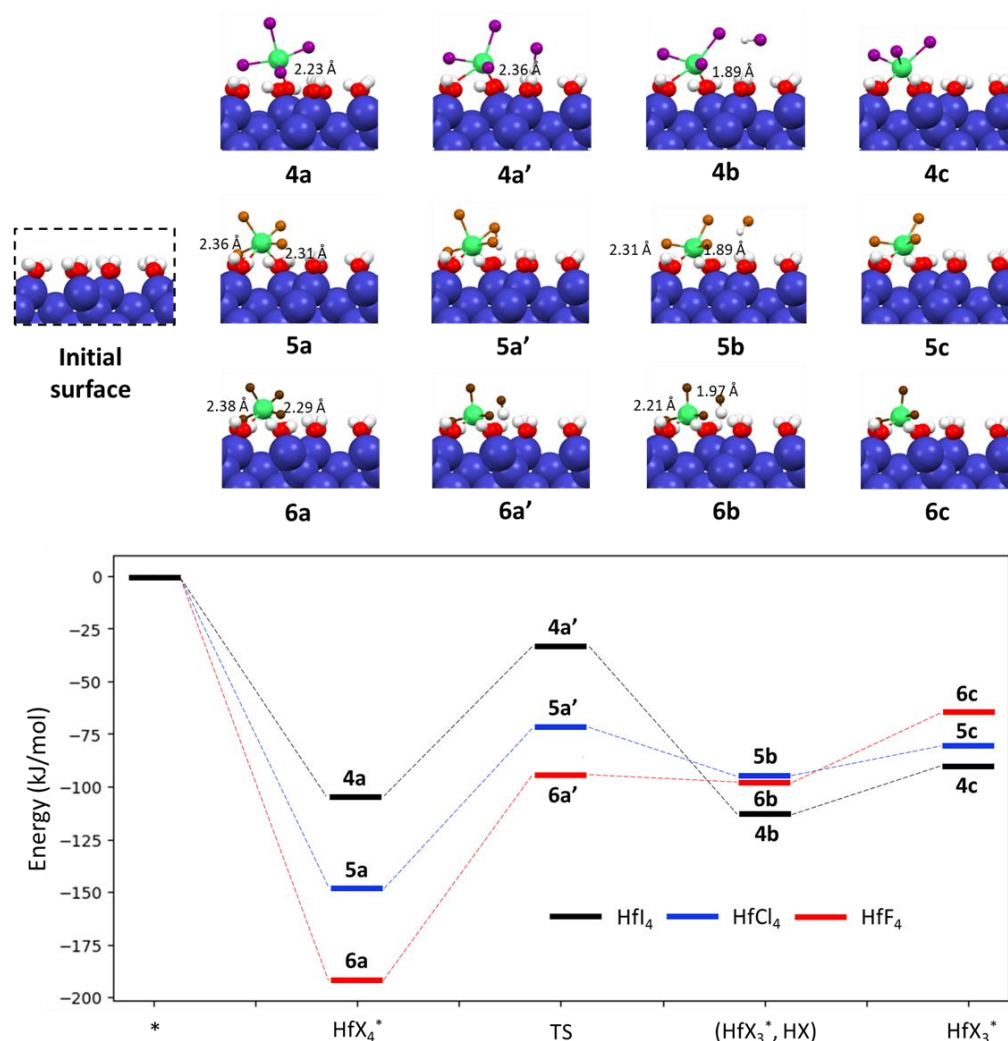


Figure 2. Reaction energy profiles in kJ/mol for chemisorption and surface reactions of hafnium halides on the fully hydroxylated Si(100) surface. Blue, red, white, gray, green, purple, orange and brown balls indicate Si, O, H, C, Hf, I, Cl, and F atoms, respectively.

At final step, free HF is released from surface with desorption energy of 30.1 kJ/mol. The product HfF₃^{*} is directly bound to surface O-atom which is formed by exchange-ligand process between HfF₄^{*} and surface OH-groups.

3.3. Chemisorption and Surface Reaction of Hafnium Amide Precursors

Hafnium amides are another family of hafnium precursors that are widely used in the HfO₂ ALD process. Hafnium amides are known to have lower thermal stabilities, but higher reactivities, compared to hafnium halides, making them suitable for use in thermal ALD processes at low temperature.

In this section, a series of hafnium amides, including tetrakis(dimethylamino) hafnium TDMAH (Hf[NMe₂]₄), tetrakis(ethylmethylamino) hafnium TEMAH (Hf[NEtMe]₄), and tetrakis(diethylamino) hafnium TDEAH (Hf[NEt₂]₄), were investigated (Me and Et stand for -CH₃ and -C₂H₅, respectively). The adsorption configurations, transition and final states, and desorption configurations of these hafnium amides on the hydroxylated Si(100) surface along with their energy profile are given in Figure 3.

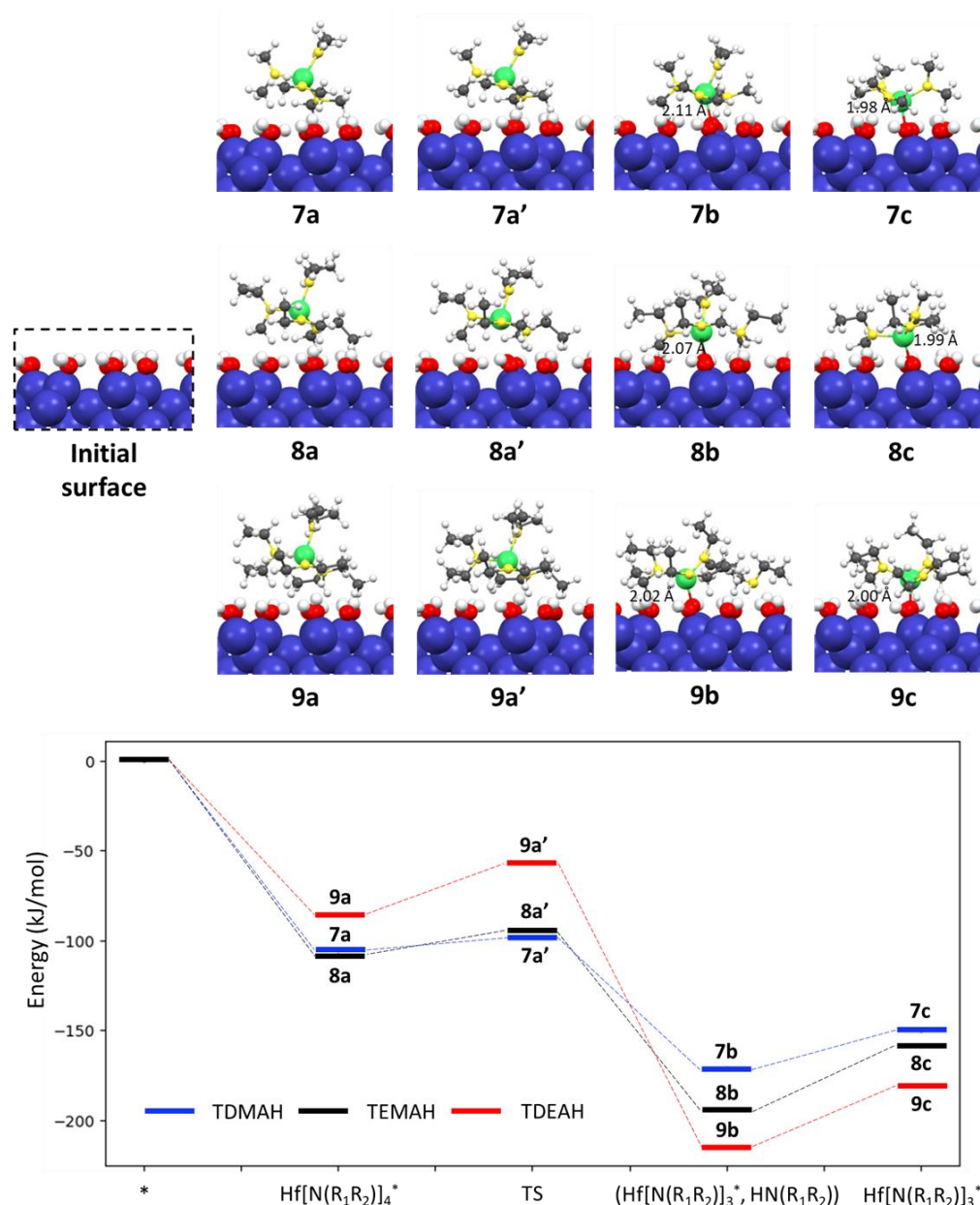


Figure 3. Reaction energy profiles in kJ/mol for chemisorption and surface reactions of hafnium amides on the fully hydroxylated Si(100) surface. Blue, red, white, gray, green and yellow balls indicate Si, O, H, C, Hf, and N atoms, respectively.

3.3.1. Tetrakis (Dimethylamino) Hafnium (TDMAH)

Our calculations demonstrate that TDMAH ($\text{Hf}[\text{NMe}_2]_4$) initially adsorbs onto the hydroxylated Si surface, forming the adsorption configuration **7a** with an adsorption energy of -104.9 kJ/mol. The Hf-O distance between the Hf atom and the surface O atoms in **7a** varies in the range from 3.51 to 3.67 Å. Subsequently, a ligand exchange reaction occurs between one of the ligands of TDMAH and nearby surface OH groups, resulting in the formation of the product **7b** (tri(dimethylamino)hafnium) ($\text{Hf}[\text{NMe}_2]_3$) through a transition state **7a'**. This reaction exhibits an exceptionally low energy barrier of only 7.1 kJ/mol and is thermodynamically favorable, with an exothermic energy of -66.1 kJ/mol. The Hf atom in **7b** retains a four-fold coordination state, binding with three remaining amino ligands and one surface O atom. After the desorption of free organic molecules HNMe_2 from **7b**, the configuration of **7c** undergoes slight changes in the Hf-O bonding length in **7d** measuring 1.98 Å, slightly shorter than the 2.11 Å in **7b**.

3.3.2. Tetrakis (Ethylmethylamino) Hafnium (TEMAH)

Our predictions, as depicted in Figure 3, also indicate relatively small differences in the adsorption configurations, of TEAMH ($\text{Hf}[\text{NEtMe}]_4$) and TDMAH precursors on the Si(100) surface. Due to the large size of the ligand -NEtMe, TEMAH only experiences physical adsorption on the OH-terminated Si(100) surface, resulting in configuration **8a**, with an adsorption energy of 107.5 kJ/mol. Chemisorption is achieved through a subsequent ligand exchange reaction between TEMAH and neighboring surface OH groups. The adsorbed TEAMH* **8a** is converted into adsorbed tri(ethylmethylamino) hafnium **8b** via a transition state **8a'** with a small activation energy of 12.8 kJ/mol. This exothermic reaction has a reaction energy of -86.9 kJ/mol. The Hf-O bonding lengths of the chemisorption configurations **8b** and **8c** are 2.07 Å and 1.99 Å, respectively, which are almost the same as those of 2.11 Å and 1.98 Å in **7b** and **7c**. At final step, molecule HNEtMe ($\text{HN}[\text{CH}_3][\text{C}_2\text{H}_5]$) is released from surface with desorption energy of 35.4 kJ/mol

Being different from our predictions, by employing a cluster model in which the Si surface is substituted by a Si_9H_{12} cluster, Wang et al. [46] demonstrated that TEAMH undergoes direct conversion into a chemisorption state, characterized by an adsorption energy of 1.42 eV. Notably, no initial adsorption state was identified in this model. The observed disparity can be attributed to the substantial size of TEAMH, whereas the cluster surface model, containing only two OH groups, is relatively diminutive. Consequently, the interaction between the surface and TEAMH was not adequately described.

3.3.3. Tetrakis (Diethylamino) Hafnium (TDEAH)

Similar to the cases of the TDMAH ($\text{Hf}[\text{NET}_2]_4$) and TEMAH precursors, TDEAH can also undergo a ligand exchange reaction to form chemisorption on the OH-terminated Si(100) surface with a relatively small energy barrier. The adsorption energy of the initially physically adsorbed configuration **9a** of TDEAH on the Si surface is -85.7 kJ/mol, which is slightly smaller than the values of -104.9 kJ/mol and -107.5 kJ/mol for TDMAH and TEMAH, respectively. This can be attributed to the fact that TDEAH is bulkier than TDMAH and TEMAH, making it more difficult to approach the Si surface. The LER that converts **9a** to the product **9b** through a transition state **9a'** has an activation energy of 28.4 kJ/mol, which is also slightly higher than that observed for TDMAH and TEMAH. However, the chemisorption configurations **9b** and **9c** exhibit bonding characteristics similar to those of TDMAH and TEMAH. The Hf-O bonding lengths in **9b** and **9c** are 2.02 Å and 2.00 Å, respectively. The molecule HNET_2 is desorbed from the surface with desorption energy of 34.4 kJ/mol.

In general, we observed that the difference in energy barriers of LERs for the three hafnium amide precursors is quite small. The activation energy of the LER converting TDMAH into tri(dimethylamino) hafnium is 7.1 kJ/mol, which is slightly lower than the value of 12.8 kJ/mol for TEMAH and 28.4 kJ/mol for TDEAH. These theoretical predictions align well with the experimental results previously reported by Hausmann et al. [74], where the temperature required for hafnium amide precursors to achieve an exactly saturating dose is 75 °C for TDMAH, 115 °C for TEMAH, and 130 °C for TDEAH

3.4. Effect of Thermal Stability and Size of Precursors on Their Reactivities

The precursors utilized in the ALD process play a pivotal role in influencing both the performance of the ALD process and the quality of the deposited films. Previous research has highlighted the significance of precursor reactivity on the substrate surface as one of the most critical factors in determining the ALD temperature window and the growth rate of the deposited materials. Precursors with higher reactivity toward the surface substrate will necessitate lower process temperatures in comparison to those with lower reactivities.

Our calculations, summarized in Table 1, show that hafnium amide precursors are more reactive than hafnium alkoxide and hafnium halide precursors for HfO_2 ALD process on hydroxylated Si(100) surface. The activation energies of the LERs between hafnium amides and surface OH groups of Si(100) surface range from 7.1 to 28.4 kJ/mol, which are

much lower than those of hafnium halides (from 71.4 kJ/mol to 97.4 kJ/mol) and hafnium alkoxides (33.0 kJ/mol to 70.2 kJ/mol). These results are consistent with experimental findings showing that the ALD process using hafnium amide precursors only requires low processing temperatures, even below 100 °C. The temperature window of the ALD process using hafnium halides and hafnium alkoxides is in the range of 250–480 °C [3].

Table 1. The adsorption energies ($\Delta E_{ads.}$), activation energies ($\Delta E_{act1.}$ for first reaction step (a to b) of all precursors and $\Delta E_{react2.}$ for second reaction step (b to c) of hafnium alkoxides), and reaction energies ($\Delta E_{react1.}$ for first reaction step (a to b) of all precursors and $\Delta E_{react2.}$ for second reaction step (b to c) of hafnium alkoxides) of hafnium precursors and desorption energy ($\Delta E_{des.}$) of byproduct (ROH for hafnium alkoxides, HX for hafnium halides, and $\text{HN}(\text{R}_1\text{R}_2)$ for hafnium amides) in kJ/mol units on the hydroxylation Si(100) surface.

Precursors	$\Delta E_{ads.}$	$\Delta E_{act1.}$	$\Delta E_{react1.}$	$\Delta E_{act2.}$	$\Delta E_{react2.}$	$\Delta E_{des.}$
Hf[OMe] ₄	−126.0	5.4	−40.9	No TS	33.0	41.0
Hf[O ⁱ Pr] ₄	−94.4	3.0	−13.8	63.8	−40.0	52.1
Hf[O ^t Bu] ₄	−92.9	70.2	64.1	34.1	−107.4	53.7
HfI ₄	−104.9	71.4	−8.3			23.1
HfCl ₄	−147.6	76.1	52.9			14.1
HfF ₄	−192.1	97.4	97.3			30.1
Hf[NMe ₂] ₄	−104.9	7.1	−66.1			20.5
Hf[NEtMe] ₄	−107.5	12.8	−86.9			35.4
Hf[NEt ₂] ₄	−85.7	28.4	−129.2			34.4

Interestingly, our above predictions also demonstrate that while the reactivities of the above amide precursors are similar, significant differences were found for the alkoxide and halide precursors. The energy barrier of ligand-exchange reaction during the chemisorption of hafnium methoxide (Hf[OMe]₄) is only 33.0 kJ/mol (**1b** → **1c**), which is much lower than the corresponding values of 63.8 kJ/mol for hafnium isopropoxide (Hf[OⁱPr]₄) and 70.2 kJ/mol for hafnium tert-butoxide (Hf[O^tBu]₄). This prediction agrees well with the early experimental results showing that the temperature window of the ALD process using hafnium isopropoxide is 250–300 °C, which is about 100 °C lower than that of the process using hafnium tert-butoxide [3]. In other way, we found that the activation energies of LERs for HfCl₄ and HfI₄ are 76.1 kJ/mol and 71.4 kJ/mol, respectively, which are lower than the value of 97.4 kJ/mol for hafnium fluoride (HfF₄).

These findings raise a question regarding whether the size and thermal stability of hafnium precursors have an impact on their reactivity and subsequent chemisorption onto the Si(100) surface. In the case of hafnium alkoxides, it is evident that hafnium methoxide exhibits higher reactivity with the OH-terminated Si(100) surface compared to hafnium isopropoxide and hafnium tert-butoxide, primarily due to the smaller size of the methoxide ligands. However, for hafnium halides, the effect of ligand size is negligible, likely due to the approximate size of halogen atoms. Thus we suppose that the thermal stability of precursors can considerably impact on their reactivities.

In order to further understand the effect of the thermal stability of precursors on their reactivity, their bond dissociation energies (BDEs) were calculated by using the isolated molecular model. BDEs, referring to the energy required to break a specific bond in a molecule and form two separate radical species, can be used as a factor of the thermal stability of a compound. By comparing the BDEs of different compounds, one can assess the relative stability of these compounds. Although a BDE value is a thermodynamic quantity, it can be used to predict reaction kinetics [75,76]. In previous studies, the BDE values were also used to gain a greater insight into the reaction mechanisms and characteristic dominant pathways of different types of reactions [77,78].

The molecular geometries of hafnium alkoxides and hafnium halides at a neutral state were optimized by using PBE0 functional and are depicted in Figure S1, while their average BDEs are given in Table S1 (Supplementary Information). It can be seen that there are

negligible differences in the BDEs of alkoxide precursors. The BDE of $\text{Hf}[\text{OMe}]_4$, $\text{Hf}[\text{O}^i\text{Pr}]_4$, and $\text{Hf}[\text{O}^t\text{Bu}]_4$ is 448 kJ/mol, 451 kJ/mol, and 454 kJ/mol, respectively. This means that the energy barrier of reaction of hafnium alkoxides on the surface is mainly effected by the size of alkoxide ligands rather than their thermal stability.

Moreover, the values presented in Table S1 demonstrate that the bond dissociation energies (BDEs) of HfI_4 , HfCl_4 , and HfF_4 are 359 kJ/mol, 487 kJ/mol, and 633 kJ/mol at the PBE0/def2sv level of theory (these BDE values are 349 kJ/mol, 475 kJ/mol, and 628 kJ/mol at the PBE0/aug-cc-pVTZ-PP), respectively. Notably, these values align in the same order as their energy barriers of ligand-exchange reactions during chemisorption on the Si(100) surface ($\text{HfI}_4 < \text{HfCl}_4 < \text{HfF}_4$). Among the hafnium halides, HfF_4 exhibits the highest thermal stability, with a remarkably high BDE of 628 kJ/mol, and it displays the highest energy barrier of 97.4 kJ/mol for chemisorption. These results suggest that, for hafnium halides with approximately similar ligand sizes, a higher thermal stability of the precursors leads to an elevated energy barrier for ligand exchange reactions on the surface. These predictions also align with previous experimental findings that reported a lower reactivity of HfCl_4 toward the Si(100) surface compared to HfI_4 [20].

4. Conclusions

In this report, we have investigated the surface reactions of a series of homoleptic hafnium precursors on the hydroxylated Si(100) surface. We have explored nine homoleptic hafnium precursors, including $\text{Hf}[\text{OMe}]_4$, $\text{Hf}[\text{O}^i\text{Pr}]_4$, $\text{Hf}[\text{O}^t\text{Bu}]_4$, HfI_4 , HfCl_4 , HfF_4 , TDMAH, TEAMH, and TDEAH. Our theoretical predictions are consistent with previously reported experimental studies, which suggest that hafnium amides are more reactive than other types of precursors. In contrast, the hafnium halides exhibit high energy barriers, whereas the hafnium alkoxides demonstrate moderate reactivity on the hydroxylated Si(100) surface.

Among alkoxide precursors, $\text{Hf}[\text{OMe}]_4$ exhibits the lowest energy barrier, while $\text{Hf}[\text{O}^t\text{Bu}]_4$ has the highest activation energy. In case of hafnium halides, HfF_4 exhibits the highest energy barrier in the first ligand exchange reaction. For hafnium amide precursors, the activation energy of TDMAH is slightly lower than compared to the other amides.

Our investigation indicate that the chemisorption and reactivity of the hafnium precursors are considerably affected by their thermal stabilities and sizes. For hafnium alkoxides, which have similar thermal stability, the size of alkoxide ligands is crucial for their chemisorption on the surface. Alternatively, for hafnium halides, whose sizes of ligands are similar, their thermal stabilities play an key role in their reactivities on the surface.

These insights not only shed light on the relationship between precursor reactivity and factors like size and thermal stability but also provide guidance for designing new heteroleptic precursors. Further investigation into heteroleptic precursors is anticipated to yield significant advancements in enhancing the performance of HfO_2 thin films in the future.

Supplementary Materials: The following supporting information can be downloaded at: <https://www.mdpi.com/article/10.3390/coatings13122094/s1>. Figure S1: The optimized geometries of hafnium alkoxides and hafnium halides obtained at PBE0 functional; Table S1: The average bond dissociation energies (BDEs) of the hafnium precursors obtained at PBE0 functional along with 6-31G(d,p) basis set for C, H, O and def2sv basis set for F, Cl, I and Hf. The values in brackets are obtained by using aug-cc-pVTZ (for F and Cl) and aug-cc-pVTZ-PP (for Hf and I) basis sets.

Author Contributions: Conceptualization, T.B.T., J.L. and H.S.; methodology, T.B.T. and H.S.; validation, T.B.T., J.L. and H.S.; formal analysis, T.B.T., J.L. and H.S.; investigation, T.B.T., J.L. and H.S.; writing—original draft preparation, T.B.T.; writing—review and editing, T.B.T., J.L. and H.S.; supervision, J.L. and H.S.; funding acquisition, H.S. All authors have read and agreed to the published version of the manuscript.

Funding: This work was supported by the National Research Foundation of Republic of Korea Grant funded by the Korean Government (MOE).

Institutional Review Board Statement: Not applicable.

Informed Consent Statement: Not applicable.

Data Availability Statement: Data are contained within the article and Supplementary Materials.

Conflicts of Interest: The authors declare no conflict of interest.

References

1. Suntola, T. Atomic layer epitaxy. *Mater. Sci. Rep.* **1989**, *4*, 261–312. [[CrossRef](#)]
2. Suntola, T.; Hyvarinen, J. Atomic layer epitaxy. *Annu. Rev. Mater. Sci.* **1985**, *15*, 177–195. [[CrossRef](#)]
3. Puurunen, R.L. A short history of atomic layer deposition: Tuomo Suntola's atomic layer epitaxy. *Chem. Vap. Depos.* **2014**, *20*, 332–344. [[CrossRef](#)]
4. Tai, T.B.; Cao, L.; Mattelaer, F.; Rampelberg, G.; Hashemi, F.S.M.; Dendooven, J.; van Ommen, J.R.; Detavernier, C.; Reyniers, M.-F. Atomic Layer Deposition of Al₂O₃ Using Aluminum Triisopropoxide (ATIP): A Combined Experimental and Theoretical Study. *J. Phys. Chem. C* **2019**, *123*, 485–494. [[CrossRef](#)]
5. Shteplyuk, I.; Yakimova, R. Special Issue "Fundamentals and Recent Advances in Epitaxial Graphene on SiC". *Appl. Sci.* **2021**, *11*, 3381. [[CrossRef](#)]
6. Elliott, S.D.; Dey, G.; Maimaiti, Y.; Ablat, H.; Filatova, E.A.; Fomengia, G.N. Modeling mechanism and growth reactions for new nanofabrication processes by atomic layer deposition. *Adv. Mater.* **2015**, *28*, 5367–5380. [[CrossRef](#)] [[PubMed](#)]
7. George, S.M. Atomic Layer Deposition: An Overview. *Chem. Rev.* **2010**, *110*, 111–131. [[CrossRef](#)]
8. Mallick, B.C.; Hsieh, C.-T.; Yin, K.-M.; Gandomi, Y.A.; Huang, K.-T. Review—On Atomic Layer Deposition: Current Progress and Future Challenges. *ECS J. Solid State Sci. Technol.* **2019**, *8*, N55–N78. [[CrossRef](#)]
9. Shahmohammadi, M.; Mukherjee, R.; Sukotjo, C.; Diwekar, U.M.; Takoudis, C.G. Recent Advances in Theoretical Development of Thermal Atomic Layer Deposition: A Review. *Nanomaterials* **2022**, *12*, 831. [[CrossRef](#)]
10. Miiikkulainen, V.; Leskela, M.; Ritala, M.; Puurunen, R.L. Crystallinity of Inorganic Films Grown by Atomic Layer Deposition: Overview and General Trends. *J. Appl. Phys.* **2013**, *113*, 021301. [[CrossRef](#)]
11. Dingemans, G.; Kessels, W.M.M. Status and prospects of Al₂O₃-based surface passivation schemes for silicon solar cells. *J. Vac. Sci. Technol. A* **2012**, *30*, 040802. [[CrossRef](#)]
12. Giannazzo, F.; Schilirò, E.; Nigro, R.L.; Roccaforte, F.; Yakimova, R. Atomic Layer Deposition of High-k Insulators on Epitaxial Graphene: A Review. *Appl. Sci.* **2020**, *10*, 2440. [[CrossRef](#)]
13. Lee, J.-C.; Oh, S.-J.; Cho, M.; Hwang, C.S.; Jung, R. Chemical structure of the interface in ultrathin HfO₂/Si films. *Appl. Phys. Lett.* **2004**, *84*, 1305–1307. [[CrossRef](#)]
14. Kim, H.; Lee, H.-B.; Maeng, W.-J. Applications of atomic layer deposition to nanofabrication and emerging nanodevices. *Thin Solid Films* **2009**, *517*, 2563–2580. [[CrossRef](#)]
15. Sandell, A.; Karlsson, P.; Richter, J.; Blomquist, J.; Uvdal, P. Surface chemistry of HfI₄ on Si(100)-(2 × 1) studied by core level photoelectron spectroscopy. *Surf. Sci.* **2007**, *601*, 917–923. [[CrossRef](#)]
16. Fedorenko, Y.; Swerts, J.; Maes, J.W.; Tois, E.; Haukka, S.; Wang, C.-G.; Wilk, G.; Delabie, A.; Dewerd, W.; De Gendt, S. Atomic Layer Deposition of Hafnium Silicate from HfCl₄, SiCl₄, and H₂O. *Electrochem. Solid-State Lett.* **2007**, *10*, H149–H152. [[CrossRef](#)]
17. Takahashi, N.; Nonobe, S.; Nakamura, T. Growth of HfO₂ films using an alternate reaction of HfCl₄ and O₂ under atmospheric pressure. *J. Solid State Chem.* **2004**, *177*, 3944–3948. [[CrossRef](#)]
18. Kukli, K.; Ritala, M.; Sajavaara, T.; Keinonen, J.; Leskela, M. Comparison of hafnium oxide films grown by atomic layer deposition from iodide and chloride precursors. *Thin Solid Films* **2002**, *416*, 72–79. [[CrossRef](#)]
19. Nonobe, S.; Takahashi, N.; Nakamura, T. Preparation of HfO₂ nano-films by atomic layer deposition using HfCl₄ and O₂ under atmospheric pressure. *Solid State Sci.* **2004**, *6*, 1217–1219. [[CrossRef](#)]
20. Aarik, J.; Aidla, A.; Kikas, A.; Käämbre, T.; Rammula, R.; Ritslaid, P.; Uustare, T.; Sammelselg, V. Effects of precursors on nucleation in atomic layer deposition of HfO₂. *Appl. Surf. Sci.* **2004**, *230*, 292–300. [[CrossRef](#)]
21. Boher, P.; Defranoux, C.; Heinrich, P.; Wolstenholme, J.; Bender, H. VUV spectroscopic ellipsometry applied to the characterization of high-k dielectrics. *Mater. Sci. Eng. B* **2004**, *109*, 64–68. [[CrossRef](#)]
22. Kang, S.-W.; Rhee, S.-W.; George, S.M. Infrared spectroscopic study of atomic layer deposition mechanism for hafnium silicate thin films using HfCl₂[N(SiMe₃)₂]₂ and H₂O. *J. Vac. Sci. Technol. A* **2004**, *22*, 2392–2397. [[CrossRef](#)]
23. Vitchev, R.; Pireaux, J.; Conard, T.; Bender, H.; Wolstenholme, J.; Defranoux, C. X-ray photoelectron spectroscopy characterisation of high-k dielectric Al₂O₃ and HfO₂ layers deposited on SiO₂/Si surface. *Appl. Surf. Sci.* **2004**, *235*, 21–25. [[CrossRef](#)]
24. Kim, H.; Saraswat, K.C.; McIntyre, P.C. Comparative Study on Electrical and Microstructural Characteristics of ZrO₂ and HfO₂ Grown by Atomic Layer Deposition. *J. Mater. Res.* **2005**, *20*, 3125–3132. [[CrossRef](#)]
25. Triyoso, D.H.; Hegde, R.I.; Gregory, R. Impact of Deposition Processes on Properties of Atomic-Layer-Deposited Hafnium Zirconate High-k Dielectrics. *Electrochem. Solid-State Lett.* **2007**, *10*, H354. [[CrossRef](#)]
26. Swerts, J.; Peys, N.; Nyns, L.; Delabie, A.; Franquet, A.; Maes, J.W.; Van Elshocht, S.; De Gendt, S. Impact of Precursor Chemistry and Process Conditions on the Scalability of ALD HfO₂ Gate Dielectrics. *J. Electrochem. Soc.* **2010**, *157*, G26–G31. [[CrossRef](#)]

27. Liu, X.; Ramanathan, S.; Longdergan, A.; Srivastava, A.; Lee, E.; Seidel, T.E.; Barton, J.T.; Pang, D.; Gordon, R.G. ALD of Hafnium Oxide Thin Films from Tetrakis(ethylmethylamino)hafnium and Ozone. *J. Electrochem. Soc.* **2005**, *152*, G213. [[CrossRef](#)]
28. Jin, H.; Oh, S.K.; Kang, H.J.; Cho, M.-H. Band gap and band offsets for ultrathin $(\text{HfO}_2)_x(\text{SiO}_2)_{1-x}$ dielectric films on Si(100). *Appl. Phys. Lett.* **2006**, *89*, 122901. [[CrossRef](#)]
29. Kim, Y.; Roh, Y.; Yoo, J.-B.; Kim, H. Characteristics of atomic layer deposition grown HfO_2 films after exposure to plasma treatments. *Thin Solid Films* **2007**, *515*, 2984–2989. [[CrossRef](#)]
30. Kirsch, P.D.; Quevedo-Lopez, M.A.; Li, H.-J.; Senzaki, Y.; Peterson, J.J.; Song, S.C.; Krishnan, S.A.; Moumen, N.; Barnett, J.; Bersuker, G.; et al. Nucleation and growth study of atomic layer deposited HfO_2 gate dielectrics resulting in improved scaling and electron mobility. *J. Appl. Phys.* **2006**, *99*, 023508. [[CrossRef](#)]
31. Park, P.K.; Roh, J.-S.; Choi, B.H.; Kang, S.-W. Interfacial Layer Properties of HfO_2 Films Formed by Plasma-Enhanced Atomic Layer Deposition on Silicon. *Electrochem. Solid-State Lett.* **2006**, *9*, F34–F37. [[CrossRef](#)]
32. Rose, M.; Bartha, J.; Endler, I. Temperature dependence of the sticking coefficient in atomic layer deposition. *Appl. Surf. Sci.* **2010**, *256*, 3778–3782. [[CrossRef](#)]
33. Senzaki, Y.; Park, S.; Chatham, H.; Bartholomew, L.; Nieveen, W. Atomic layer deposition of hafnium oxide and hafnium silicate thin films using liquid precursors and ozone. *J. Vac. Sci. Technol. A* **2004**, *22*, 1175–1181. [[CrossRef](#)]
34. Son, S.Y.; Kumar, P.; Cho, H.; Min, K.J.; Kang, C.J.; Singh, R.K. An evaluation of thermal stability of TiB_2 metal gate on Hf silicate for p-channel metal oxide semiconductor application. *Appl. Phys. Lett.* **2008**, *92*, 172106. [[CrossRef](#)]
35. Wang, Y.; Dai, M.; Ho, M.-T.; Wielunski, L.S.; Chabal, Y.J. Infrared characterization of hafnium oxide grown by atomic layer deposition using ozone as the oxygen precursor. *Appl. Phys. Lett.* **2007**, *90*, 022906. [[CrossRef](#)]
36. Won, S.-J.; Kim, J.-Y.; Choi, G.-J.; Heo, J.; Hwang, C.S.; Kim, H.J. The formation of an almost full atomic monolayer via surface modification by N_2O -plasma in atomic layer deposition of ZrO_2 thin films. *Chem. Mater.* **2009**, *21*, 4374–4379. [[CrossRef](#)]
37. Kamiyama, S.; Miura, T.; Nara, Y. Electrical properties of ultrathin HfO_2 films for replacement metal gate transistors, fabricated by atomic layer deposition using $\text{Hf}(\text{N}(\text{CH}_3)(\text{C}_2\text{H}_5))_4$ and O_3 . *Appl. Phys. Lett.* **2005**, *87*, 132904. [[CrossRef](#)]
38. Tai, T.B.; Son, J.; Shin, H. A theoretical study of the atomic layer deposition of HfO_2 on Si(1 0 0) surfaces using tetrakis(ethylmethylamino) hafnium and water. *Appl. Surf. Sci.* **2023**, *612*, 155702. [[CrossRef](#)]
39. Kim, J.C.; Heo, J.S.; Cho, Y.S.; Moon, S.H. Atomic layer deposition of an HfO_2 thin film using $\text{Hf}(\text{O}-i\text{Pr})_4$. *Thin Solid Films* **2009**, *517*, 5695–5699. [[CrossRef](#)]
40. Kukli, K.; Ritala, M.; Leskelä, M.; Sajavaara, T.; Keinonen, J.; Jones, A.; Roberts, J. Atomic layer deposition of hafnium dioxide films using hafnium bis(2-butanolate)bis(1-methoxy-2-methyl-2-propanolate) and water. *Chem. Vap. Depos.* **2003**, *9*, 315–320. [[CrossRef](#)]
41. Rauwel, E.; Clavel, G.; Willinger, M.; Rauwel, P.; Pinna, N. Non-aqueous routes to metal oxide thin films by atomic layer deposition. *Angew. Chem.* **2008**, *120*, 3648–3651. [[CrossRef](#)]
42. Niinistö, J.; Putkonen, M.; Niinistö, L.; Stoll, S.L.; Kukli, K.; Sajavaara, T.; Ritala, M.; Leskelä, M. Controlled growth of HfO_2 thin films by atomic layer deposition from cyclopentadienyl-type precursor and water. *J. Mater. Chem.* **2005**, *15*, 2271–2275. [[CrossRef](#)]
43. Dezelah, C.L.; Niinistö, J.; Kukli, K.; Munnik, F.; Lu, J.; Ritala, M.; Leskelä, M.; Niinistö, L. The atomic layer deposition of HfO_2 and ZrO_2 using advanced metallocene precursors and H_2O as the oxygen source. *Chem. Vap. Depos.* **2008**, *14*, 358–365. [[CrossRef](#)]
44. Sibanda, D.; Oyinbo, S.T.; Jen, T.-C. A review of atomic layer deposition modelling and simulation methodologies: Density functional theory and molecular dynamics. *Nanotechnol. Rev.* **2022**, *11*, 1332–1363. [[CrossRef](#)]
45. Ren, J.; Zhang, Y.-T.; Zhang, D.W. Density functional theoretical study of initial stage of HfO_2 atomic layer deposition on hydroxylated SiO_2 surface. *J. Mol. Struct. Theochem* **2007**, *803*, 23–28. [[CrossRef](#)]
46. Chen, W.; Sun, Q.-Q.; Xu, M.; Ding, S.-J.; Zhang, D.W.; Wang, L.-K. Atomic Layer Deposition of Hafnium Oxide from Tetrakis(ethylmethylamino)hafnium and Water Precursors. *J. Phys. Chem. C* **2007**, *111*, 6495–6499. [[CrossRef](#)]
47. Cortez-Valadez, M.; Fierro, C.; Farias-Mancilla, J.; Vargas-Ortiz, A.; Flores-Acosta, M.; Ramírez-Bon, R.; Enriquez-Carrejo, J.; Soubervielle-Montalvo, C.; Mani-Gonzalez, P. Comparison of HfCl_4 , HfI_4 , TEMA-Hf, and TDMA-Hf as precursors in early growing stages of HfO_2 films deposited by ALD: A DFT study. *Chem. Phys.* **2016**, *472*, 81–88. [[CrossRef](#)]
48. Mui, C.; Musgarve, C.B. Atomic layer deposition of HfO_2 using alkoxides as precursors. *J. Phys. Chem. B* **2004**, *108*, 15150–15164. [[CrossRef](#)]
49. D’Acunto, G.; Tsyshkevsky, R.; Shayesteh, P.; Gallet, J.J.; Bournel, F.; Rochet, F.; Pinsard, I.; Timm, R.; Head, A.R.; Kuklja, M.; et al. Biomolecular reaction mechanism in the amido complex-based atomic layer deposition of HfO_2 . *Chem. Mater.* **2003**, *35*, 529–538. [[CrossRef](#)]
50. Kresse, G.; Joubert, D. From ultrasoft pseudopotentials to the projector augmented-wave method. *Phys. Rev. B* **1999**, *59*, 1758–1775. [[CrossRef](#)]
51. Kresse, G.; Furthmüller, J. Efficiency of ab-initio total energy calculations for metals and semiconductors using a plane-wave basis set. *Comput. Mater. Sci.* **1996**, *6*, 15–50. [[CrossRef](#)]
52. Kresse, G.; Furthmüller, J. Efficient iterative schemes for ab initio total-energy calculations using a plane-wave basis set. *Phys. Rev. B* **1996**, *54*, 11169–11186. [[CrossRef](#)] [[PubMed](#)]
53. Blöchl, P.E. Projector augmented-wave method. *Phys. Rev. B* **1994**, *50*, 17953–17979. [[CrossRef](#)] [[PubMed](#)]
54. Perdew, J.P.; Burke, K.; Ernzerhof, M. Generalized gradient approximation made simple. *Phys. Rev. Lett.* **1996**, *77*, 3865–3868. [[CrossRef](#)] [[PubMed](#)]

55. Henkelman, G.; Uberuaga, B.P.; Jónsson, H. A climbing image nudged elastic band method for finding saddle points and minimum energy paths. *J. Chem. Phys.* **2000**, *113*, 9901–9904. [[CrossRef](#)]
56. Henkelman, G.; Jónsson, H. Improved tangent estimate in the nudged elastic band method for finding minimum energy paths and saddle points. *J. Chem. Phys.* **2000**, *113*, 9978–9985. [[CrossRef](#)]
57. Monkhorst, H.J.; Pack, J.D. Special points for Brillouin-zone integrations. *Phys. Rev. B* **1976**, *13*, 5188–5192. [[CrossRef](#)]
58. Grimme, S.; Antony, J.; Ehrlich, S.; Krieg, H. A consistent and accurate ab initio parametrization of density functional dispersion correction (DFT-D) for the 94 elements H–Pu. *J. Chem. Phys.* **2010**, *132*, 154104–154119. [[CrossRef](#)]
59. Momma, K.; Izumi, F. VESTA 3 for three-dimensional visualization of crystal, volumetric and morphology data. *J. Appl. Crystallogr.* **2011**, *44*, 1272–1276. [[CrossRef](#)]
60. Macrae, C.F.; Sovago, I.; Cottrell, S.J.; Galek, P.T.A.; McCabe, P.; Pidcock, E.; Platings, M.; Shields, G.P.; Stevens, J.S.; Towler, M.; et al. Mercury 4.0: From visualization to analysis, design and prediction. *J. Appl. Crystallogr.* **2020**, *53*, 226–235. [[CrossRef](#)]
61. Frisch, M.J. (Ed.) *Gaussian 16, Revision C.01*; Gaussian, Inc.: Wallingford, CT, USA, 2016.
62. Adamo, C.; Barone, V. Toward reliable density functional methods without adjustable parameters: The PBE0 model. *J. Chem. Phys.* **1999**, *110*, 6158–6170. [[CrossRef](#)]
63. Petersson, G.A.; Bennett, A.; Tensfeldt, T.G.; Al-Laham, M.A.; Shirley, W.A.; Mantzaris, J. A complete basis set model chemistry. I. The total energies of closed-shell atoms and hydrides of the first-row elements. *J. Chem. Phys.* **1988**, *89*, 2193–2218. [[CrossRef](#)]
64. Weigend, F.; Ahlrichs, R. Balanced basis sets of split valence, triple zeta valence and quadruple zeta valence quality for H to Rn: Design and assessment of accuracy. *Phys. Chem. Chem. Phys.* **2005**, *7*, 3297–3305. [[CrossRef](#)] [[PubMed](#)]
65. Kendall, R.A.; Dunning, T.H., Jr.; Harrison, R.J. Electron Affinities of the First-Row Atoms Revisited. Systematic Basis Sets and Wave Functions. *J. Chem. Phys.* **1992**, *96*, 6796–6806. [[CrossRef](#)]
66. Woon, D.E.; Dunning, T.H., Jr. Gaussian Basis Sets for Use in Correlated Molecular Calculations. III. The atoms aluminum through argon. *J. Chem. Phys.* **1993**, *98*, 1358–1371. [[CrossRef](#)]
67. Figgen, D.; Peterson, K.A.; Dolg, M.; Stoll, H. Energy-consistent pseudopotentials and correlation consistent basis sets for the 5d elements Hf–Pt. *J. Chem. Phys.* **2009**, *130*, 164108. [[CrossRef](#)] [[PubMed](#)]
68. Peterson, K.A.; Figgen, D.; Goll, E.; Stoll, H.; Dolg, M. Systematically convergent basis sets with relativistic pseudopotentials. II. Small-core pseudopotentials and correlation consistent basis sets for the post-*d* group 16–18 elements. *J. Chem. Phys.* **2003**, *119*, 11113–11123. [[CrossRef](#)]
69. Peterson, K.A.; Shepler, B.C.; Figgen, D.; Stoll, H. On the Spectroscopic and Thermochemical Properties of ClO, BrO, IO, and Their Anions. *J. Phys. Chem. A* **2006**, *110*, 13877–13883. [[CrossRef](#)]
70. Pritchard, B.P.; Altarawy, D.; Didier, B.T.; Gibson, T.D.; Windus, T.L. New Basis Set Exchange: An Open, Up-to-date Resource for the Molecular Sciences Community. *J. Chem. Inf. Model.* **2019**, *59*, 4814–4820. [[CrossRef](#)]
71. Feller, D. The role of databases in support of computational chemistry calculations. *J. Comput. Chem.* **1996**, *17*, 1571–1586. [[CrossRef](#)]
72. Schuchardt, K.L.; Didier, B.T.; Elsethagen, T.; Sun, L.; Gurumoorthi, V.; Chase, J.; Li, J.; Windus, T.L. Basis Set Exchange: A Community Database for Computational Sciences. *J. Chem. Inf. Model.* **2007**, *47*, 1045–1052. [[CrossRef](#)] [[PubMed](#)]
73. Chemcraft—Graphical Software for Visualization of Quantum Chemistry Computations. Version 1.8, Build 682. Available online: <http://www.chemcraftprog.com> (accessed on 1 December 2023).
74. Hausmann, D.M.; Kim, E.; Becker, J.; Gordon, R.G. Atomic layer deposition of hafnium and zirconium oxides using metal amide precursors. *Chem. Mater.* **2002**, *14*, 4350–4358. [[CrossRef](#)]
75. John, P.C.S.; Guan, Y.; Kim, Y.; Kim, S.; Paton, R.S. Prediction of organic homolytic bond dissociation enthalpies at near chemical accuracy with sub-second computational cost. *Nat. Commun.* **2020**, *11*, 2328. [[CrossRef](#)] [[PubMed](#)]
76. Gani, T.Z.H.; Kulik, H.J. Understanding and breaking scaling relations in single-site catalysis: Methane to methanol conversion by Fe^{IV}=O. *ACS Catal.* **2018**, *8*, 975–986. [[CrossRef](#)]
77. Kim, S.; Fioroni, G.M.; Park, J.-W.; Robichaud, D.J.; Das, D.D.; John, P.C.S.; Lu, T.; McEnally, C.S.; Pfefferle, L.D.; Paton, R.S.; et al. Experimental and theoretical insight into the soot tendencies of the methylcyclohexene isomers. *Proc. Combust. Inst.* **2019**, *37*, 1083–1090. [[CrossRef](#)]
78. Gallegos, L.C.; Luchini, G.; John, P.C.S.; Kim, S.; Paton, R.S. Importance of engineered and learned molecular representations in predicting organic reactivity, selectivity, and chemical properties. *Acc. Chem. Res.* **2021**, *54*, 827–836. [[CrossRef](#)]

Disclaimer/Publisher’s Note: The statements, opinions and data contained in all publications are solely those of the individual author(s) and contributor(s) and not of MDPI and/or the editor(s). MDPI and/or the editor(s) disclaim responsibility for any injury to people or property resulting from any ideas, methods, instructions or products referred to in the content.